Journal of Science and Transport Technology
Journal homepage: https://jstt.vn/index.php/en

Forecasting Deep-Seated Landslide Displacements Using Machine Learning and Automated Monitoring Data

Viet-Tien Nguyen[1,2], Trong-Tai Nguyen[1], Mai Nguyen Thi[1], Yen Hoang Hai[1], Lien Vy Thi Hong[1], Do Minh Ngoc[3], Indra Prakash[4], Tran Van Phong[1,2*]

[1]Institute of Earth Sciences, Vietnam Academy of Science and Technology, 68 Huynh Thuc Khang, Hanoi, Vietnam. Email: nvtien@ies.vast.vn, tainguyenhd2210@gmail.com, ntmai@ies.vast.vn, yenhh11@gmail.com, lienvy@ies.vast.vn, tphong1617@gmail.com.

[2]Graduate University of Science and Technology, Vietnam Academy of Science and Technology, 18 Hoang Quoc Viet, Hanoi, Vietnam.

[3]Geotechnical and Artificial Intelligence research group, University of Transport Technology, Hanoi 100000, Vietnam. Email: ngocdm@utt.edu.vn

[4]Formerly Dy. Director General, Geological Survey of India, Gujarat, India. Email: indra52prakash@gmail.com

Article info
Type of article:
Original research paper

DOI:
https://doi.org/10.58845/jstt.utt.2025.en.5.4.87-106

***Corresponding author:**
Email address:
tphong1617@gmail.com

Received: 05/10/2025
Received in Revised Form: 07/11/2025
Accepted: 12/11/2025

Abstract: Deep-seated landslides are slope failures where the primary sliding surface extends beyond the soil mantle into weathered or intact bedrock, involving large volumes and slow displacement rates. Forecasting their displacements is challenging due to complex hydrological, geotechnical, and climatic interactions. This study develops a machine learning framework for short-term displacement forecasting at 6 m depth using hourly automated monitoring data from a tectonically active landslide in Lam Dong Province, Vietnam. Three models, Gradient Boosting (GB), Support Vector Regression (SVR), and Multilayer Perceptron Regression (MLPR), were trained on 16 hydrometeorological and geotechnical variables from January 2021 to November 2024. Among them, MLPR achieved the best performance (R^2 = 0.920; MAE = 0.036 mm; MAPE = 1.57%), surpassing GB (R^2 = 0.891) and SVR (R^2 = 0.873). Residual and partial dependence analyses confirmed the robustness and interpretability of MLPR, identifying precipitation, pore water pressure, and volumetric water content as dominant predictors. The results demonstrate that integrating multi-sensor real-time data with ML improves displacement forecasting accuracy and timeliness, enhancing early-warning and mitigation strategies. While this model is site-specific, it provides a scalable foundation for hybrid ML–physics approaches and multi-site ensemble learning, enabling generalization across diverse geomorphic conditions.

Keywords: deep-seated landslides; displacement forecasting; machine learning; automated monitoring; early warning systems.

1. Introduction

Landslides, particularly deep-seated types, represent one of the most destructive geohazards worldwide, responsible for billions of dollars in

economic losses and thousands of fatalities each year [1-3]. Deep-seated landslides are characterized by sliding surfaces located below the root zone, often extending into weathered or intact bedrock at depths greater than 5–10 m. These failures typically involve large volumes, slow deformation rates, and complex hydro-geomechanical processes at depth [4, 5]. Their impacts are most severe in tectonically active mountainous terrains where fractured rock masses, steep slopes, and intense rainfall accelerated by climate change trigger pore pressure buildup and progressive slope instability [5].

Forecasting the displacement of such deep-seated landslides remains a major challenge due to the nonlinear and multivariate interactions among rainfall infiltration, groundwater fluctuation, soil moisture, and temperature-driven effects [6]. Conventional approaches, such as the Limit Equilibrium Method (LEM) or analytical slip-surface models, assume static parameters and fail to capture transient environmental responses, thus limiting their predictive capability under dynamic hydrological conditions [6, 7]. Although field instrumentation such as inclinometers and extensometers provides valuable displacement measurements, they are typically site-specific, require frequent manual readings, and lack the temporal resolution necessary for real-time forecasting [8, 9].

The emergence of soft computing and machine learning (ML) has significantly advanced landslide research by enabling the discovery of complex, nonlinear relationships among multiple environmental factors [10, 11]. Ensemble algorithms such as Gradient Boosting (GB) and Support Vector Regression (SVR) have shown promise in susceptibility mapping and displacement prediction [12]. More recently, neural network-based models, including Multilayer Perceptrons (MLPs) and convolutional neural networks (CNNs), have captured nonlinear dependencies between hydrological triggers and displacement behavior [13].

Despite these advances, critical knowledge gaps persist. First, there has been limited use of high-frequency, real-time multi-sensor monitoring data to train predictive models, reducing the ability to capture rapid subsurface responses [14]. Second, many models overlook temporal dependence and lag effects among hydrological variables, increasing the risk of overfitting and reducing robustness [15-17]. Third, most approaches remain black-box frameworks with limited interpretability, constraining their operational use in early-warning systems [18].

To address these gaps, the present study develops a comparative machine learning framework using Gradient Boosting (GB), Support Vector Regression (SVR), and Multilayer Perceptron Regression (MLPR) models trained on hourly, multi-sensor monitoring data from a deep-seated landslide in Lam Dong Province, Central Highlands, Vietnam. The monitoring system integrates extensometers, inclinometers, piezometers, GNSS sensors, and rainfall gauges, providing sixteen hydrometeorological and geotechnical parameters for model training and validation from January 2021 to November 2024.

The **objectives** of this study are to:

(i) preprocess and analyze high-frequency automated monitoring data for displacement forecasting at 6 m depth;

(ii) develop and optimize multiple ML models to evaluate predictive performance through robust diagnostics; and

(iii) interpret the influence of key parameters on displacement behavior to enhance physical understanding and model transparency.

The novelty of this research lies in the integration of continuous, multi-sensor real-time data with advanced machine learning models to improve both accuracy and interpretability in deep-seated landslide displacement forecasting. The findings contribute to operational landslide early-warning systems by providing a scalable, data-driven framework applicable to other tectonically

active mountainous regions under changing climatic conditions.

2. Automated observation station at the studied landslide site

The studied landslide is located in Lam Dong Province, Central Highlands, Vietnam, a region characterized by steep terrain, fractured bedrock, and annual rainfall exceeding 2000 mm [19]. This deep-seated landslide, exhibiting slow progressive movements, poses a significant threat to local infrastructure and communities. The site was selected as it represents a typical landslide-prone environment under combined geological and hydrometeorological stresses.

To ensure continuous and high-resolution monitoring, an automated observation station was established at the site (Fig. 1). The system integrates multiple geotechnical and hydrological sensors designed to measure slope deformation and subsurface hydrodynamics in real time. The main components include:

- Inclinometers and extensometers to record horizontal and vertical displacements along the slope;
- Piezometers to measure groundwater and pore-water pressures influencing shear strength;
- GNSS receivers for continuous surface displacement tracking;
- Rain gauges to quantify precipitation, the dominant external trigger; and
- Soil temperature and volumetric water content sensors to capture thermo-hydrological variations controlling slope response.

The sensors are connected through a central data logger powered by solar panels with battery backup, ensuring uninterrupted operation during adverse weather conditions. Measurements are automatically recorded at hourly intervals and transmitted via GSM or satellite network to a central server. This allows real-time access for analysis, quality control, and early-warning alerts. Data redundancy is maintained through dual storage—locally at the site and remotely at the monitoring center.

Fig. 1 schematically illustrates the layout and functioning of the automated observation station. The diagram shows sensor placement at various depths within the landslide mass, data acquisition and logging components, transmission paths, and the flow of information to remote servers for model integration and analysis.

Compared with traditional manual measurements, the automated system offers significant advantages in accuracy, continuity, and rapid detection of abnormal displacements. Continuous high-frequency data capture ensures that short-term variations and precursory signals preceding movement acceleration are recorded, which manual observations often miss. The system also reduces human error and improves responsiveness, forming a critical input for the machine learning models developed in this study.

Regular calibration and maintenance were performed to ensure sensor stability and data accuracy. Protective casings were installed to shield sensors from extreme rainfall and temperature fluctuations. These improvements have enabled the collection of reliable, long-term, and noise-reduced datasets that underpin the predictive framework presented in this research.

3. Methodology and Materials

3.1. Study Site and Data Acquisition

The study site is located at 12°2′3″N 108°25′40″E in Lac Duong District, Lam Dong Province, Central Highlands, Vietnam, within a tectonically active terrain characterized by fractured sandstone–shale sequences and weathered clay-rich soils. The site has a humid subtropical climate, with mean annual rainfall exceeding 2000 mm, primarily concentrated between May and October. Continuous creep-type displacement of a deep-seated landslide (~6–20 m thick) has been observed since 2019.

To establish a clear framework for classifying the type and scale of slope movements analyzed in this study, the distinction between shallow and

deep-seated landslides was defined based on depth thresholds and characteristic features reported in previous literature. Table 1 summarizes the commonly adopted depth criteria and typical geotechnical and hydrological characteristics associated with each category, which provided the basis for delineating the deep-seated landslides investigated in the present research.

These classification criteria were subsequently used to guide the selection of monitoring locations, interpretation of subsurface displacement data, and the development of machine learning models tailored specifically for forecasting deep-seated landslide movements.

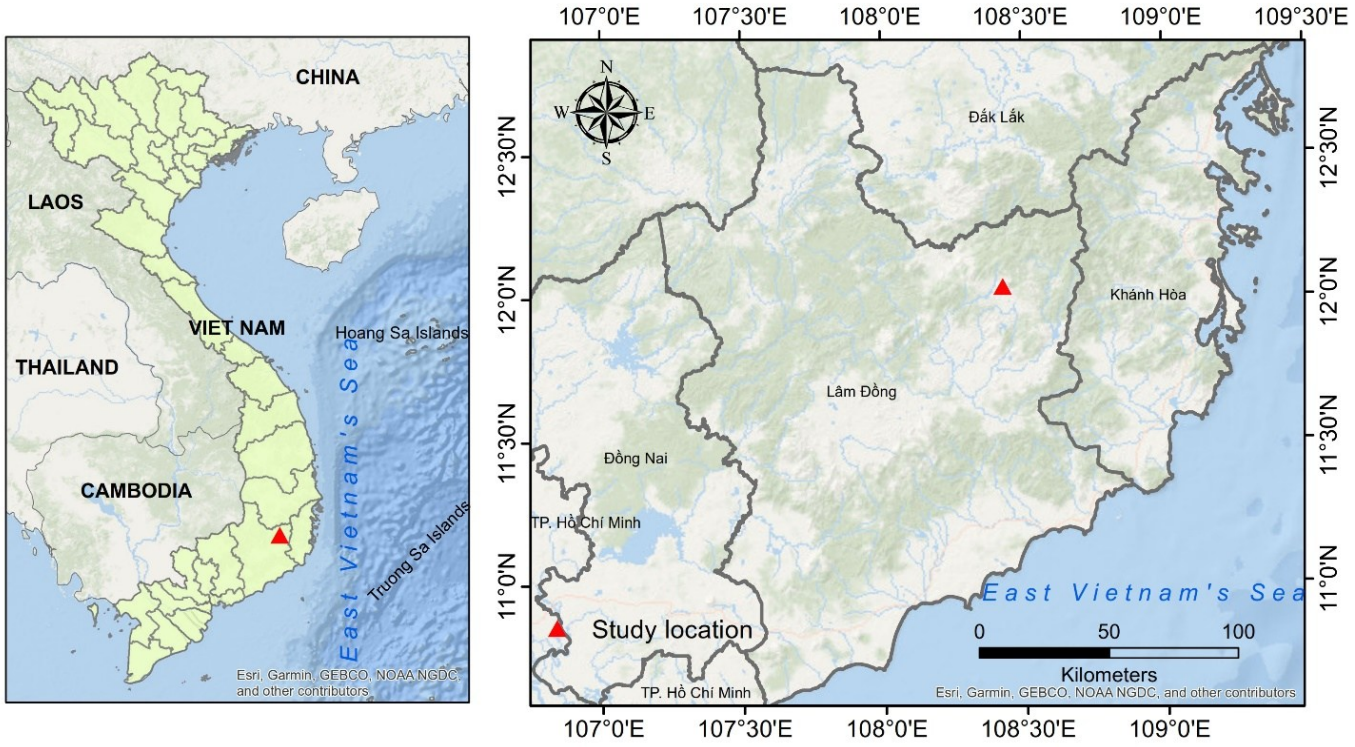

Fig. 1. The location of the monitored landslide station

Table 1. Depth Thresholds and Typical Characteristics Reported in Previous Studies

Classification	Threshold / Depth Criterion	Typical Characteristics
Shallow landslides	Sliding surface within soil mantle or weathered bedrock; typically a few decimetres up to several metres (e.g. < ~1-5 m) below ground surface. (1Library)	Rapid response to rainfall (short-duration, high intensity), small volumes, more frequent, failure often translational or planar, occurs in upper soil layers, often within the rooting zone; higher velocity. (Gelogia)
Deep-seated landslides	Sliding surface deeper than shallow threshold; often > ~5-10 m (variously given); extends into weathered or intact bedrock below the rooting zone. Some papers use >10 m as a threshold. (Gelogia)	Larger volumes, slow to moderate rates of displacement, longer response times (lags) to hydrological triggers, complex movement (rotational, translational, or compound), often involve subsurface hydrology (pore water pressure), deeper shear surfaces, and potential for large deformation over long periods [20].

Data used in this study were collected from the automated observation station described in Section 2, operating continuously from January 2021 to November 2024. Hourly data acquisition produced a high-resolution dataset of approximately 35,000 records. The dataset

contains 16 predictor variables covering meteorological, hydrological, and geotechnical domains, with the target variable being displacement (mm) measured at 6 m depth (near the shear zone).

The input variables include:

PREC: Precipitation (mm), representing rainfall as a primary external trigger for soil saturation and pore water pressure increase.

MEM1–MEM5: Voltage readings (V) from extensometers at depths of 17 m to 6 m, detecting strain or displacement in the soil and rock mass to track slope deformation.

AVP1–AVP2: Average pore water pressure (mH_2O) at two locations, influencing shear strength by reducing effective stress.

AVT1–AVT2: Average temperature (°C) at two soil depths, affecting moisture content, chemical weathering, and mechanical strength.

P1–P2: Pressure difference (mH_2O) between two points in the landslide mass, indicating shifts in slope stability.

VWC: Volumetric water content (m^3/m^3), measuring soil moisture levels that reduce cohesion and trigger saturation.

EC: Electrical conductivity (dS/m), reflecting soil salinity and moisture changes for slope stability assessment.

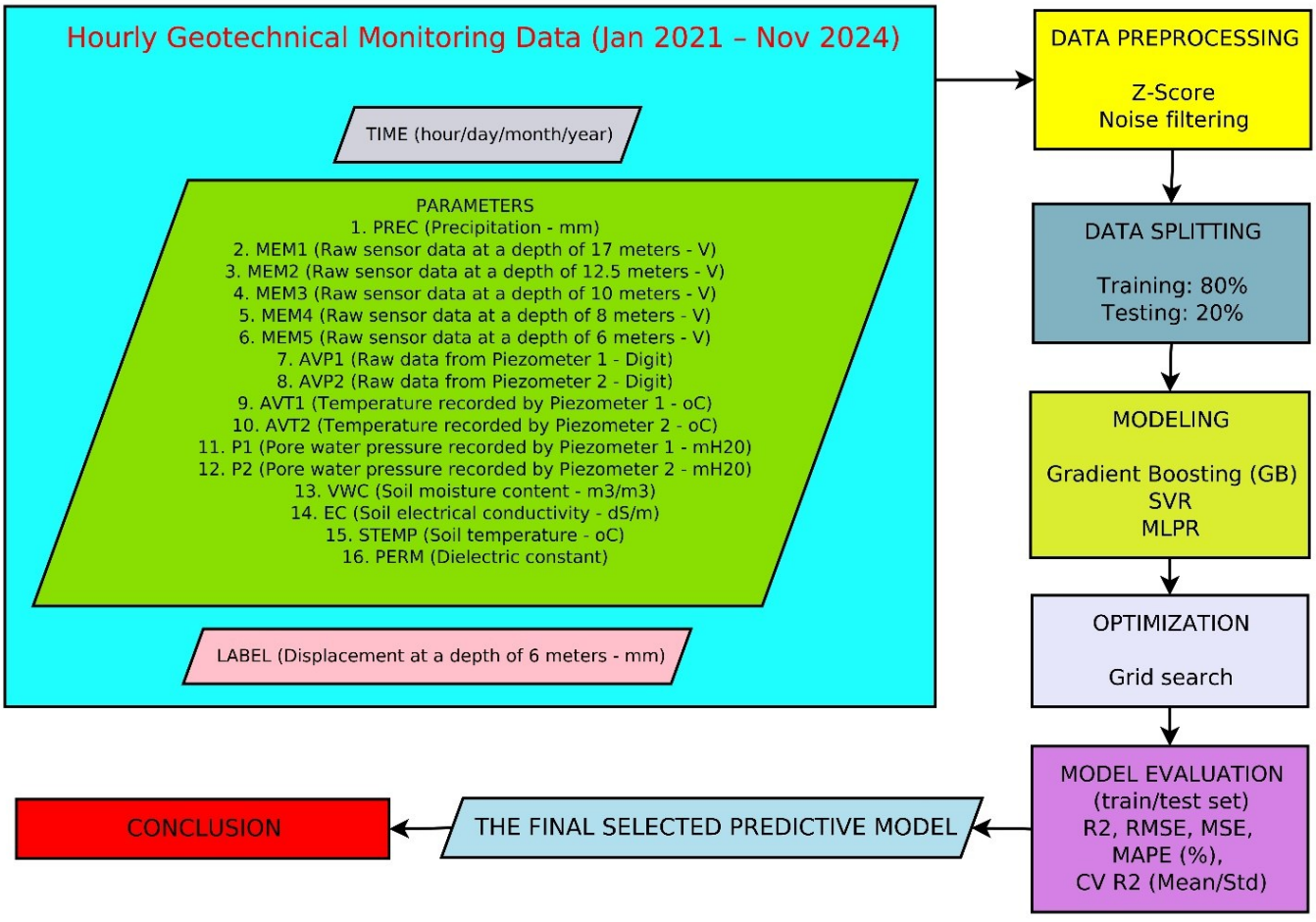

Fig. 2. Diagram of the research process

STEMP: Soil temperature (°C), influencing microbial activity, compaction, moisture retention, and freeze-thaw cycles.

PERM: Dielectric constant (dimensionless), indicating soil permeability and water transmission rates that impact pore pressure buildup.

These variables were selected based on established geotechnical and hydrological principles, with physical linkages to slope stability: rainfall (PREC) elevates pore pressures, extensometer readings (MEM1–MEM5) enable early movement detection, and moisture indicators

(VWC, PERM) signal saturation risks. Temperature (AVT1–AVT2, STEMP) and pressure differentials (P1–P2) provide contextual insights into thermo-hydro-mechanical dynamics, while EC tracks compositional shifts.

Fig. 2 illustrates the research workflow, highlighting the sensor-driven, depth-stratified dataset structure. It emphasizes hourly collection for tracking saturation dynamics, with raw data preprocessed via Z-score normalization to the [-1,1] range for scale invariance and Savitzky-Golay filtering to preserve transients while mitigating noise.

3.2. Data Preprocessing and Analysis

To ensure reliability, a structured data preprocessing workflow was implemented. Outliers were removed using the 1.5× IQR method (<2% anomalies), followed by Z-score normalization to the [−1, 1] range. The Savitzky–Golay smoothing filter reduced noise while preserving short-term dynamics. Correlation analysis confirmed inter-variable consistency and guided feature retention.

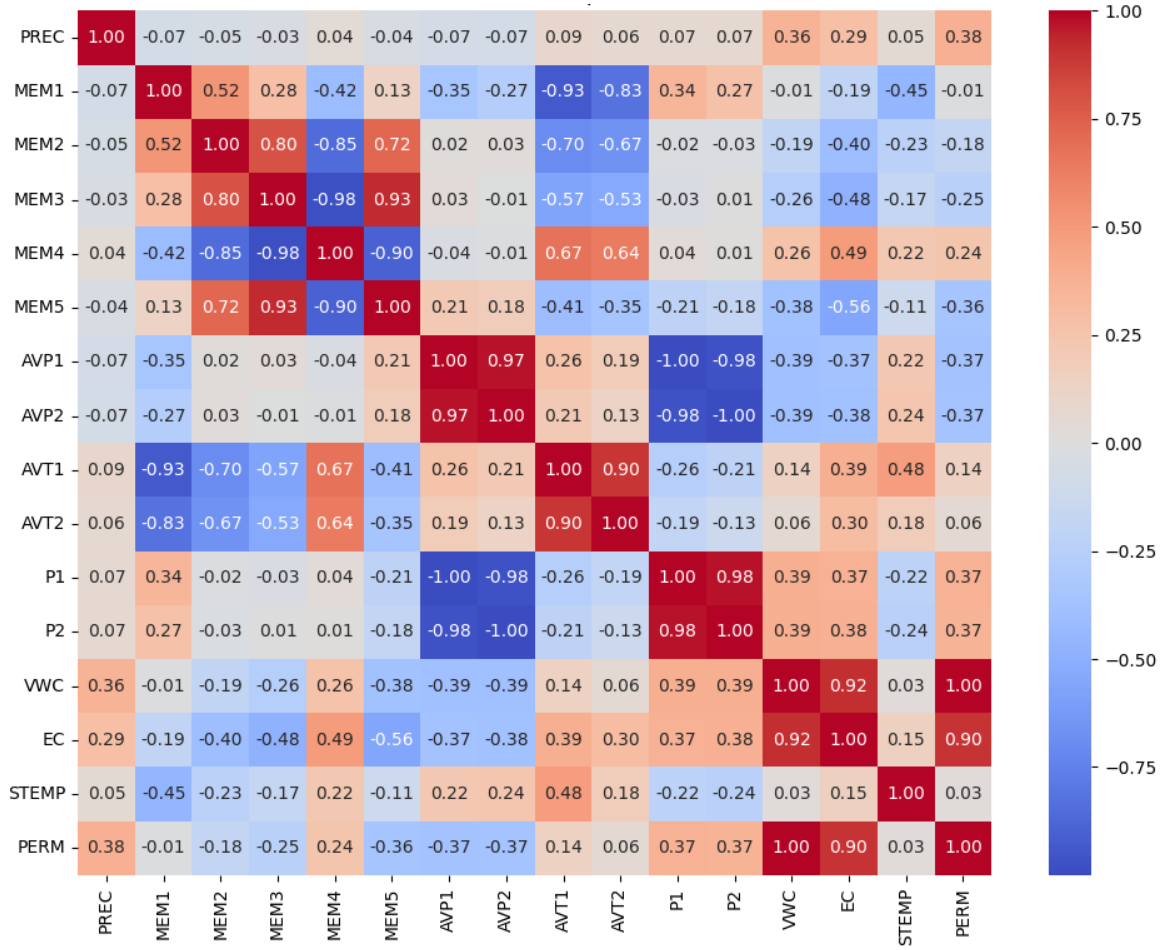

Fig. 3. Correlation Matrix of Input Variables

A correlation matrix was computed to assess inter-variable dependencies and potential multicollinearity. Highly correlated variables (e.g., AVP1–AVP2: ρ = 0.97; VWC–PERM: 0.90) were retained because the selected models (GB, SVR, MLPR) include built-in regularization mechanisms that mitigate overfitting from redundant inputs. The correlation analysis also revealed physical relationships between hydrological and geotechnical parameters, confirming data consistency.

The dataset was divided into training (80%) and testing (20%) subsets using a chronological time-series split that preserves the temporal structure. This ensures that training precedes testing in time, avoiding data leakage and maintaining forecasting realism. The 80/20 ratio was selected after evaluating several splits (70/30,

60/40), where 80/20 provided the most stable generalization without excessive data fragmentation. Only the training dataset was used to determine optimal model hyperparameters through cross-validation and grid search.

Fig. 3 depicts the correlation matrix, revealing clusters of interdependency: strong positive correlations among MEM sensors (e.g., MEM2–MEM5: 0.93) and negative ones (e.g., MEM3–MEM4: -0.98) indicate subsurface stress propagation; piezometer variables (AVP1–AVP2, P1–P2: >0.98) confirm groundwater linkage; and moisture-related features (VWC–PERM: 0.90) validate hydrological consistency. Precipitation (PREC) shows weak correlations (-0.1 to +0.1), underscoring nonlinear, lagged effects, while STEMP exhibits moderate ties (e.g., with AVT1: 0.48). This analysis informed feature retention and regularization to manage redundancy without dimensionality reduction.

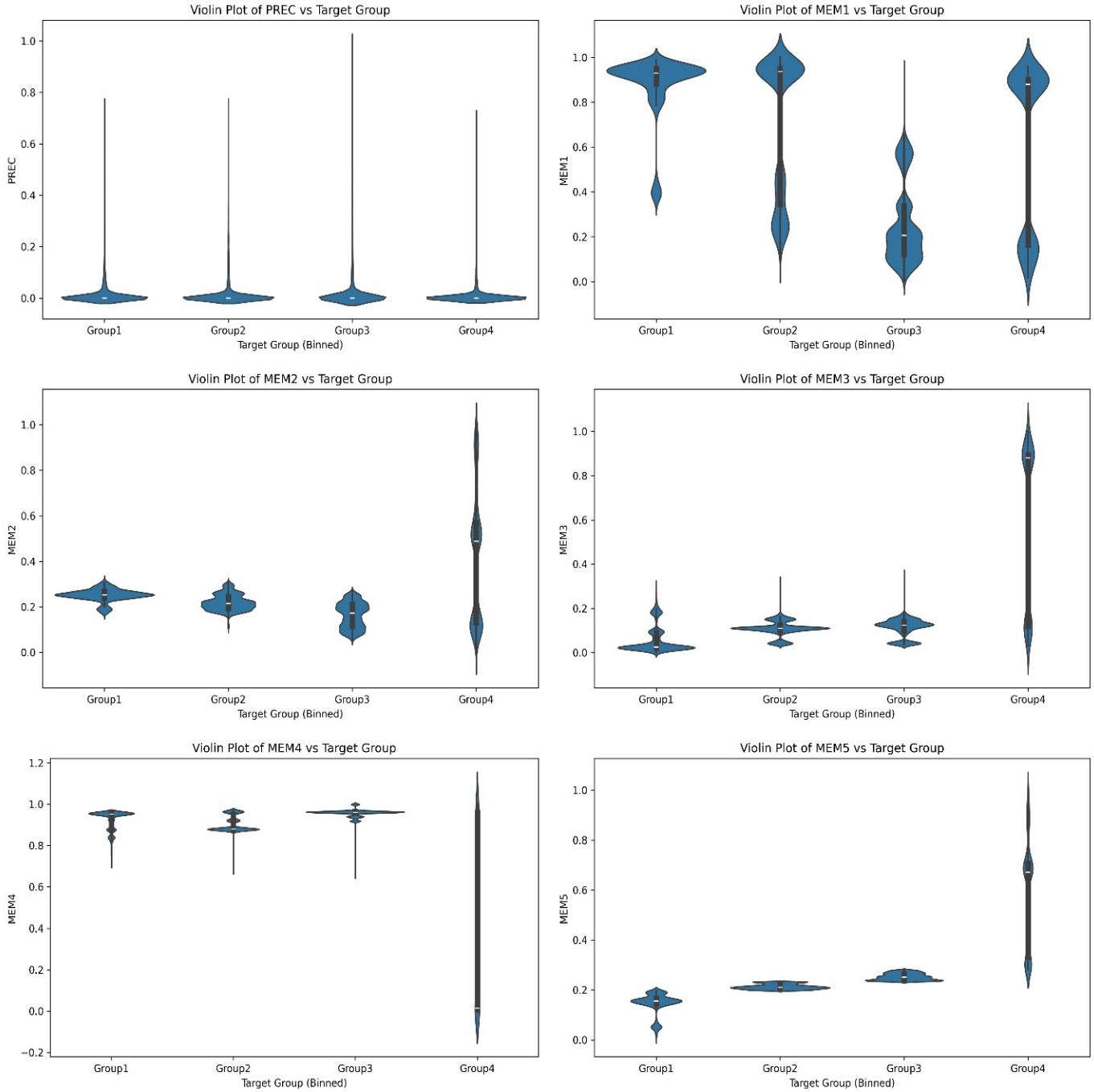

Fig. 4. Violin plots of variables vs predictive target

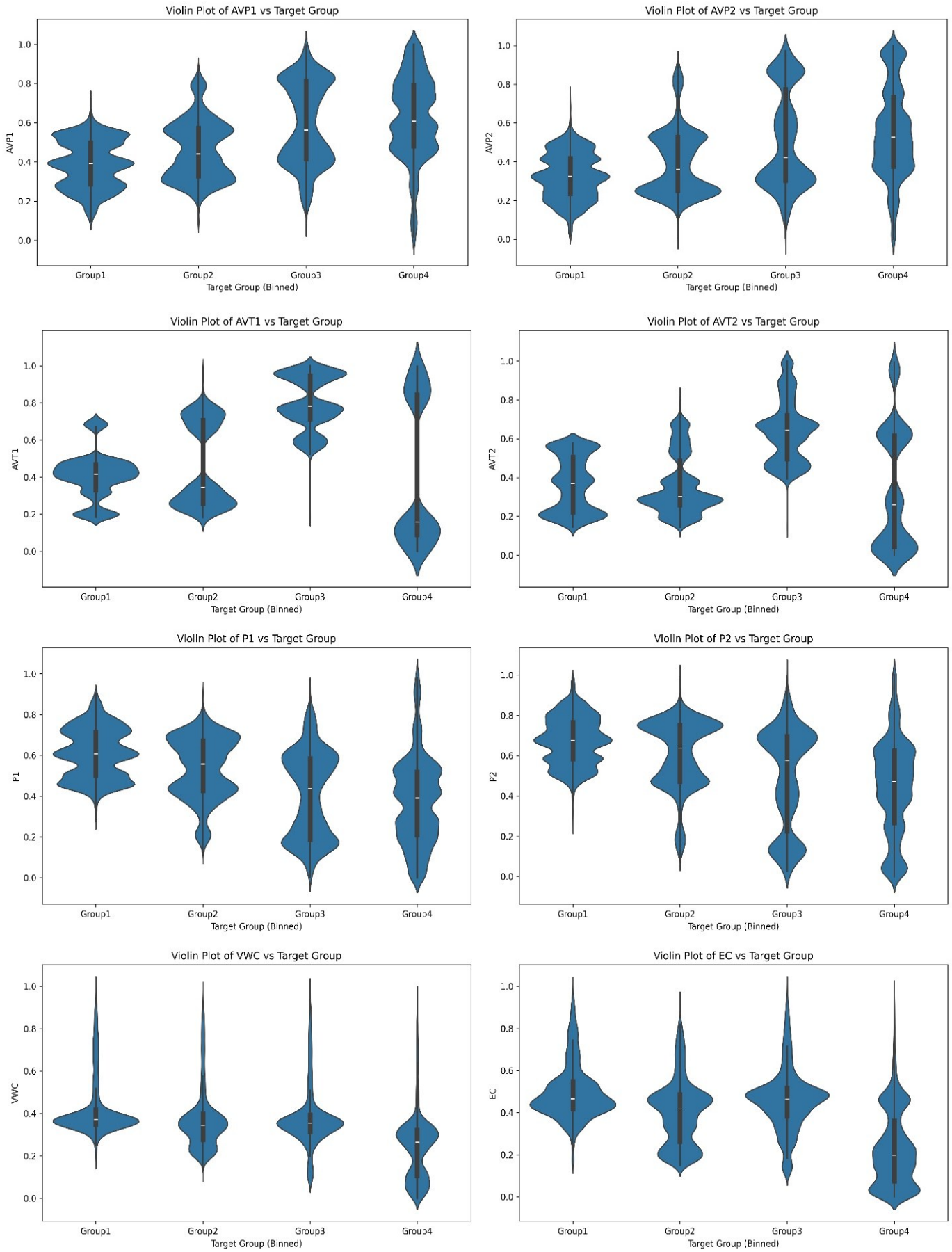

Fig. 4. (continued)

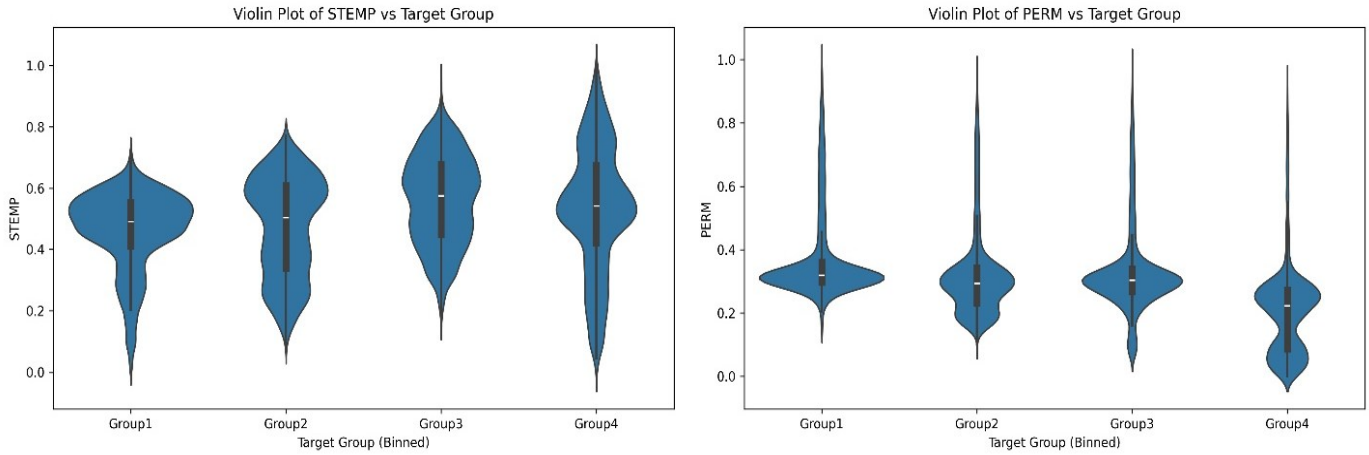

Fig. 4. (continued)

Fig. 4 presents violin plots stratified by displacement severity (four quartiles, Group 1–4), affirming hydrological dominance: monotonic escalations in PREC, MEM1–MEM5, AVP1–AVP2, P1–P2, VWC, and PERM (e.g., tighter, elevated distributions in Group 4 for MEM4–MEM5 and PERM) highlight their predictive relevance for saturation-driven failures. In contrast, EC and temperature variables (AVT1–AVT2, STEMP) show overlapping, flat distributions, suggesting secondary roles. These visualizations prioritize meteorological and hydrological features, supporting the model's focus on hydrodynamics and rainfall stress. Groups 1–4 in Fig. 3 correspond to quartile-based categories of displacement magnitude, with Group 1 representing the lowest 25% and Group 4 the highest 25% of displacement values. This classification enables visualization of how hydrological and geotechnical parameters vary with displacement intensity.

3.3. Machine Learning Models

Three regression models were developed and compared: Gradient Boosting (GB), Support Vector Regression (SVR), and Multilayer Perceptron Regression (MLPR). Model implementation was performed using Python (v3.11) with the scikit-learn and TensorFlow libraries. Hyperparameters were optimized via exhaustive grid search with 5-fold cross-validation, ensuring stability and generalization.

3.3.1. Gradient Boosting (GB)

Gradient Boosting (GB), introduced by Friedman (2001) as a greedy function approximation via sequential decision trees, aggregates weak learners to minimize residuals, excelling in nonlinear feature interactions relevant to landslide kinematics [21]. Each iteration fits a shallow tree to negative gradients of the loss function (mean squared error, MSE), updating predictions as:

$$F_m(x)=F_{m-1}(x)+\eta\cdot h_m(x) \quad (1)$$

where

$$h_m(x)=\arg\min_h \sum_i L(y_i,F_{m-1}(x_i)+h(x_i)) \quad (2)$$

Here, L is the MSE loss function, η=0.1 is the learning rate, $n_{estimators}$ = 200, and max_depth = 5 (Table 2). The loss is:

$$L=\frac{1}{N}\sum(y_i-\hat{y}_i^{(m)})^2 \quad (3)$$

and the tree targets:

$$r_{im}=-\left[\frac{\partial L(y_i,F(x_i))}{\partial F(x_i)}\right]_{F(x)=F_{m-1}(x_i)} \quad (4)$$

Advantages include high accuracy on complex data like rainfall-pore pressure interactions and reduced overfitting via shrinkage (η). Drawbacks encompass computational expense for large datasets and hyperparameter sensitivity, though regularization mitigates risks. In landslide forecasting, GB captures intricate environmental dependencies, outperforming traditional methods.

3.3.2. Support Vector Regression (SVR)

Support Vector Regression (SVR), adapted

from SVM by Vapnik (1995), approximates targets within an ε-insensitive margin using the kernel trick for nonlinearity [22]. It minimizes regularized risk:

$$\min_{w,b,\xi,\xi^*} \frac{1}{2}\|w\|^2+C\sum_i(\xi_i+\xi_i^*) \quad (5)$$

subject to:

$$|y_i-(w^T\phi(x_i)+b)|\leq\epsilon+\xi_i,\xi_i,\xi_i^*\geq 0 \quad (6)$$

with RBF kernel $K(x_i,x_j)=\exp(-\gamma\|x_i-x_j\|^2)$(C=10, ε=0.1, γ=0.1; Table 2). This balances complexity and errors via slack variables, mapping data to higher dimensions for linear separation of nonlinear patterns.

SVR robustly handles landslide nonlinearity (e.g., rainfall-soil interactions) and resists overfitting in noisy, high-dimensional data. However, it is computationally intensive for large datasets and sensitive to outliers beyond ε, requiring careful tuning. For deep-seated displacements, SVR excels in modeling interdependent factors like moisture and slope characteristics, enhancing real-time prediction accuracy.

3.3.3. Multilayer Perceptron Regression (MLPR)

Multilayer Perceptron Regression (MLPR), rooted in neural networks, employs backpropagation for hierarchical feature abstraction [23]. It features input-hidden-output layers with Tanh activation:

$$z^{(l)}=\sigma(W^{(l)}a^{(l-1)}+b^{(l)}) \quad (7)$$

Minimized on MSE:

$$L=\frac{1}{N}\sum(y_i-\hat{y}_i)^2 \quad (8)$$

(2 hidden layers: 64-32 neurons, max_iter=500; Table 2). Forward propagation computes:

$$a^{(l)}=\sigma(W^{(l)}a^{(l-1)}+b^{(l)}) \quad (9)$$

enabling nonlinear mappings via gradient descent.

MLPR captures complex landslide patterns (e.g., multi-factor interactions) and supports real-time inference post-training. Limitations include data hunger to prevent overfitting, high computational demands, and low interpretability. In this context, MLPR facilitates the abstraction of kinematics from diverse inputs, aiding risk mitigation.

Table 2 summarizes optimized parameters: GB (max_depth=5, n_estimators=200, learning_rate=0.1) for balanced boosting; SVR (C=10, ε=0.1, γ=0.1) for nonlinear regularization; MLPR (Tanh, hidden_layers=(64,32), max_iter=500) for compact abstraction. Grid search ensured dataset-specific tuning.

Table 2. Optimized model parameters obtained through grid search

Parameters	Models		
	GB	SVR	MLPR
Max_depth	5		
N_estimators	200		
Learning rate	0.1		
C		10	
Epsilon		0.1	
gamma		0.1	
Activation			Tanh
Hiden layers			2 layers (64, 32)
Max_iterations			500

3.4. Model Evaluation and Interpretability

Model performance was evaluated using standard regression metrics: coefficient of determination (R^2), mean squared error (MSE), mean absolute error (MAE), and mean absolute percentage error (MAPE). Additional diagnostics, including residual distribution plots, R^2 scatter plots, and partial dependence plots (PDPs), were used to assess prediction quality and interpret model behavior.

Diagnostics including residual plots/histograms (Figs. 8–13), R^2 scatter plots (Figs. 14–16), and partial dependence plots (PDPs; Fig. 17) via scikit-learn.

To avoid overfitting, models were validated through 5-fold cross-validation on the training dataset. Residual analyses and PDPs were used to ensure that the models captured nonlinear hydrological relationships rather than spurious noise.

This rigorous pipeline enables traceable, regulatory-adoptable predictions, emphasizing diagnostic depth for landslide early warning.

4. Results and Discussion

The comparative performance of ML models is summarized in Table 3. MLPR achieved the highest predictive accuracy (R^2 = 0.920; MAE = 0.036 mm; MAPE = 1.57%), outperforming GB and SVR.

4.1. Model Performance and Comparative Accuracy

The predictive performance of the three models, Multilayer Perceptron Regression (MLPR), Gradient Boosting (GB), and Support Vector Regression (SVR), was evaluated using R^2, MSE, MAE, and MAPE metrics (Table 3).

MLPR achieved the best overall performance, with a testing R^2 of 0.920, MAE of 0.036 mm, and MAPE of 1.57%, outperforming GB (R^2 = 0.891, MAE = 0.022 mm, MAPE = 1.162%) and SVR (R^2 = 0.873, MAE = 0.043 mm, MAPE = 2.004%). The results demonstrate that MLPR successfully captures complex nonlinear dependencies between hydrological and geotechnical variables, providing robust generalization across unseen data.

During training, all models showed very high R^2 values (~0.99), indicating excellent fitting. However, such near-perfect results can reflect potential overfitting if models memorize noise rather than learn generalizable patterns. Residual analysis and cross-validation were therefore applied to verify true generalization capability (Section 4.3).

Table 3. Performance evaluation of the models

Model	Training			Testing				Cross Validation	
	R2	MSE	MAE	R2	MSE	MAE	MAPE	Mean	Std
MLPR	0.999	8.17E-05	0.007	0.920	0.002	0.036	1.570	0.666	0.493
GB	0.999	2.88E-07	0.0004	0.891	0.003	0.022	1.162	0.656	0.499
SVR	0.993	0.002	0.041	0.873	0.004	0.043	2.004	0.519	0.521

All three models were trained and tested on the same dataset, ensuring fair comparison. Hyperparameter optimization was based only on the training subset, eliminating data leakage and enhancing model validity.

4.2. Temporal Prediction Pattern

Time-series comparisons between actual and predicted displacements at 6 m depth (mm) are shown in Figs. 5–7. The MLPR model (Fig. 7) provided the most accurate alignment with observed displacements, reproducing both short-term oscillations and long-term creep with minimal phase lag. GB (Fig. 5) closely tracked overall trends but slightly underestimated peak values during high-rainfall periods (e.g., March 2024), reflecting its smoothing effect. SVR (Fig. 6) successfully modeled gradual displacement changes but attenuated sharp accelerations following rainfall events.

However, testing predictions (green line, early to late 2024) displayed mild smoothing and underestimation of peak amplitudes (e.g., March 2024 surge), resulting in a conservative trajectory during the post-peak decline. This reflects GB's tendency toward overfitting noise in training while maintaining directional accuracy (R^2 = 0.891), ideal

for trend-based early warnings but less responsive to extreme transients.

SVR's predictions (Fig. 6) revealed a smoother fit across both datasets, with training outputs closely tracing actual displacements without spurious oscillations, thanks to its regularization and ε-margin. The model adeptly reproduced long-term trends and seasonal oscillations, showing only subtle lags during high-variance episodes (e.g., sharp spikes attenuated to milder bumps). On testing data, SVR generalized well, paralleling gradual changes with near-overlap but exhibiting inertial responses to abrupt shifts, aligning with its testing R^2 of 0.873. This low-pass filtering effect enhances stability against outliers but may underestimate sudden rainfall-induced accelerations, a trade-off evident in its higher MAPE.

MLPR (Fig. 7) achieved the closest overall correspondence, with training predictions virtually indistinguishable from actuals, filtering minor noise while preserving short- and long-term dynamics. Testing outputs tracked major rises and falls effectively, though subtle phase shifts and modest under-/overestimations at peaks/troughs emerged, indicative of hierarchical abstraction without severe overfitting (testing R^2 = 0.920). MLPR's depth enabled superior capture of nonlinear kinematics, outperforming GB's smoothing and SVR's attenuation, particularly in volatile periods.

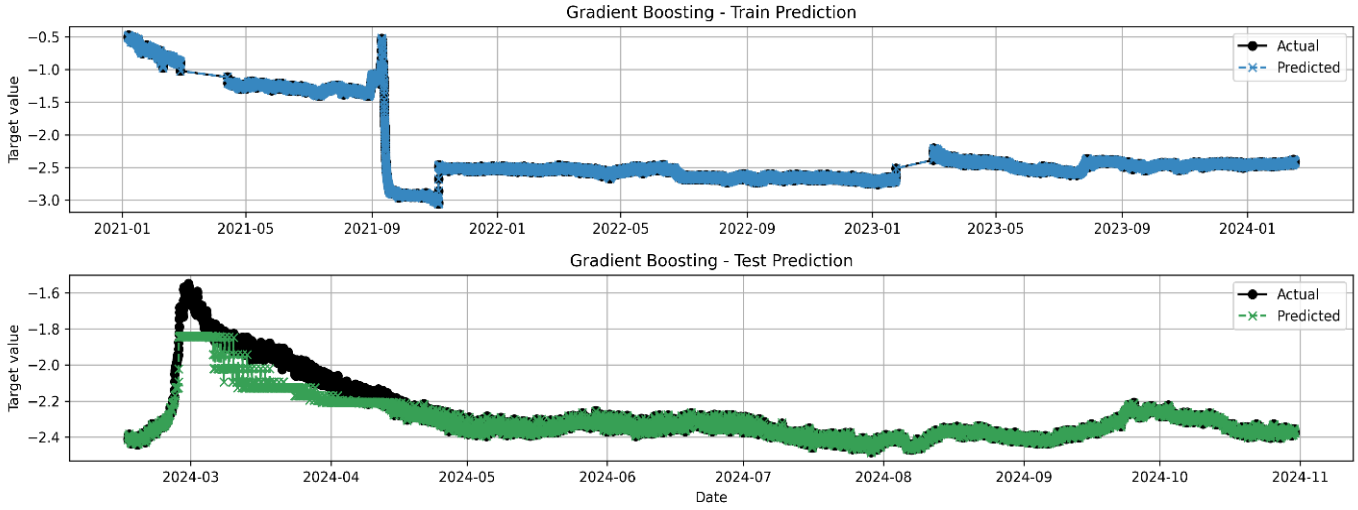

Fig. 5. Prediction plots of 6-meter depth displacement using the Gradient Boosting model on training and testing datasets

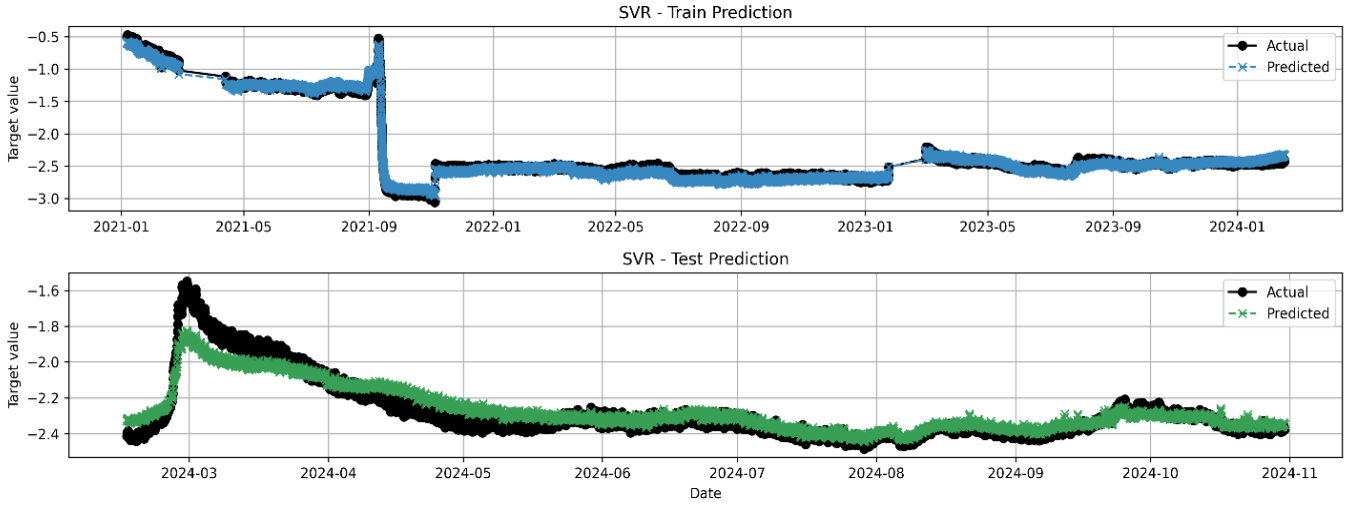

Fig. 6. Prediction plots of 6-meter depth displacement using the Support Vector Regression model on training and testing datasets

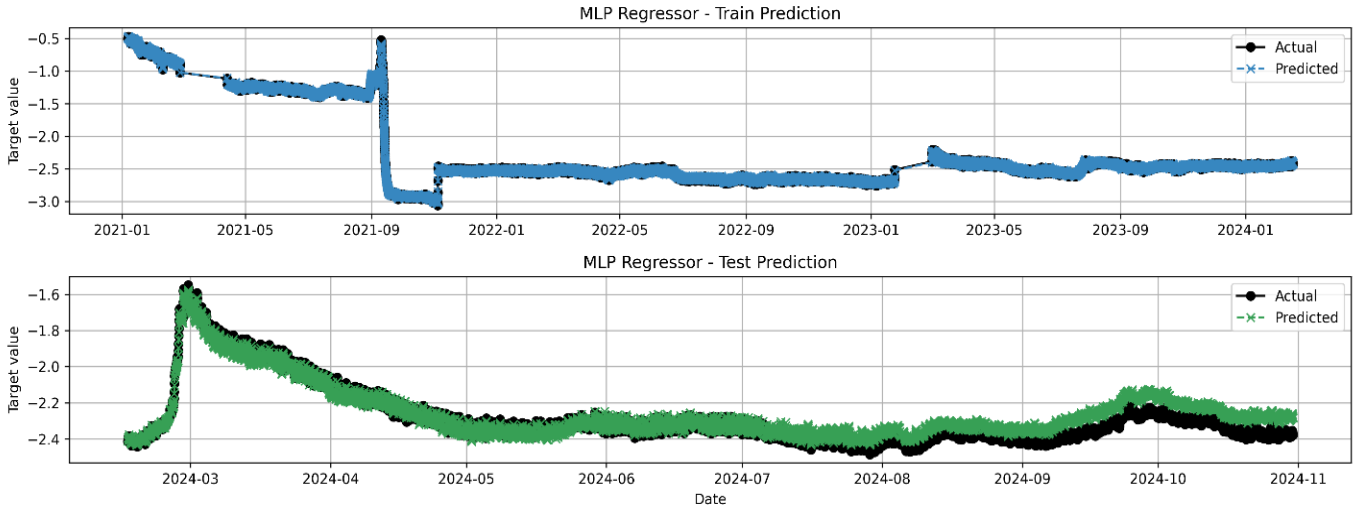

Fig. 7. Prediction plots of 6-meter depth displacement using the Multilayer Perception Regression model on training and testing datasets

Overall, MLPR provided the most realistic temporal dynamics, making it particularly suitable for early-warning applications requiring timely and responsive prediction behavior.

These visualizations underscore MLPR's edge in transient modeling, essential for proactive landslide mitigation, while highlighting ensemble (GB) and kernel-based (SVR) models' roles in stable trend forecasting.

4.3. Residual Analysis and Overfitting Evaluation

Residual distribution plots (Figs. 8–13) and scatter diagrams (Figs. 14–16) confirmed that model errors were centered around zero with no significant bias. The MLPR residuals were narrow and symmetrical, indicating low variance and minimal heteroscedasticity. In contrast, GB exhibited slightly broader tails on testing data, suggesting limited overfitting that remained within acceptable bounds. SVR residuals were more dispersed, reflecting underfitting during sharp or extreme displacement changes. Cross-validation yielded average R^2 values of 0.666 (MLPR), 0.656 (GB), and 0.519 (SVR) with small standard deviations (<0.5), confirming the stability of the models across data folds. These outcomes indicate that MLPR achieved a sound balance between flexibility and generalization, whereas GB was more conservative, and SVR suffered from over-regularization of complex transients.

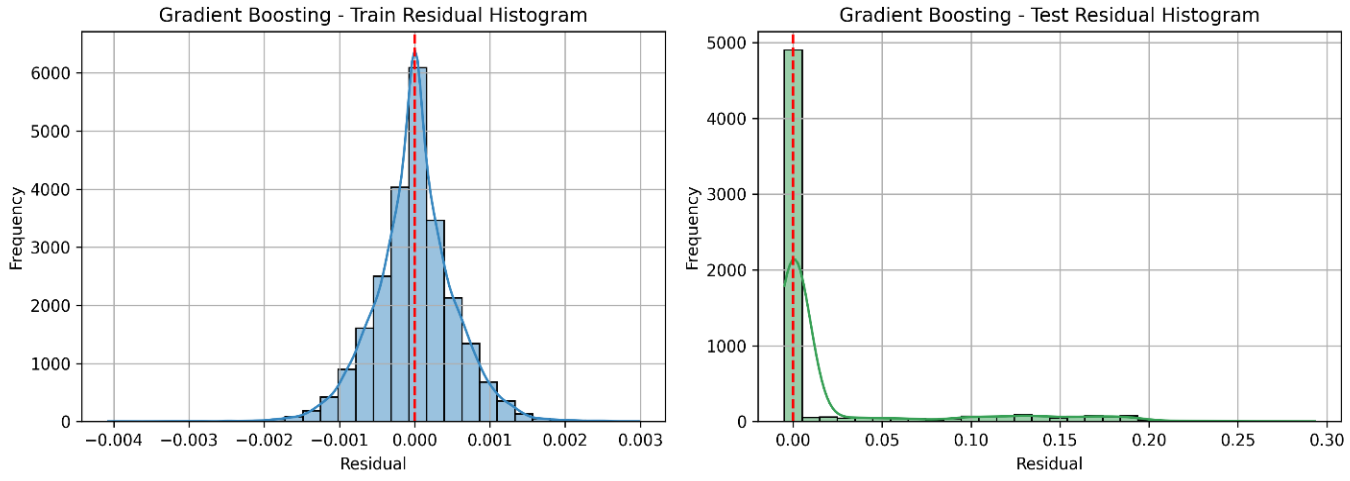

Fig. 8. Residual Frequency histogram of the Gradient Boosting model

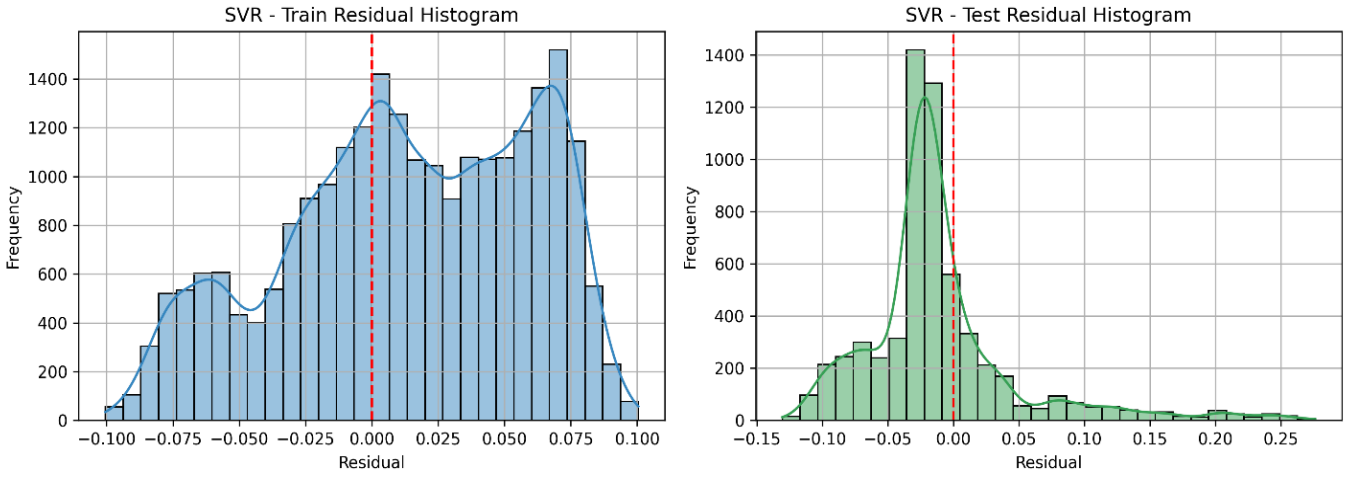

Fig. 9. Residual Frequency histogram of the SVR model

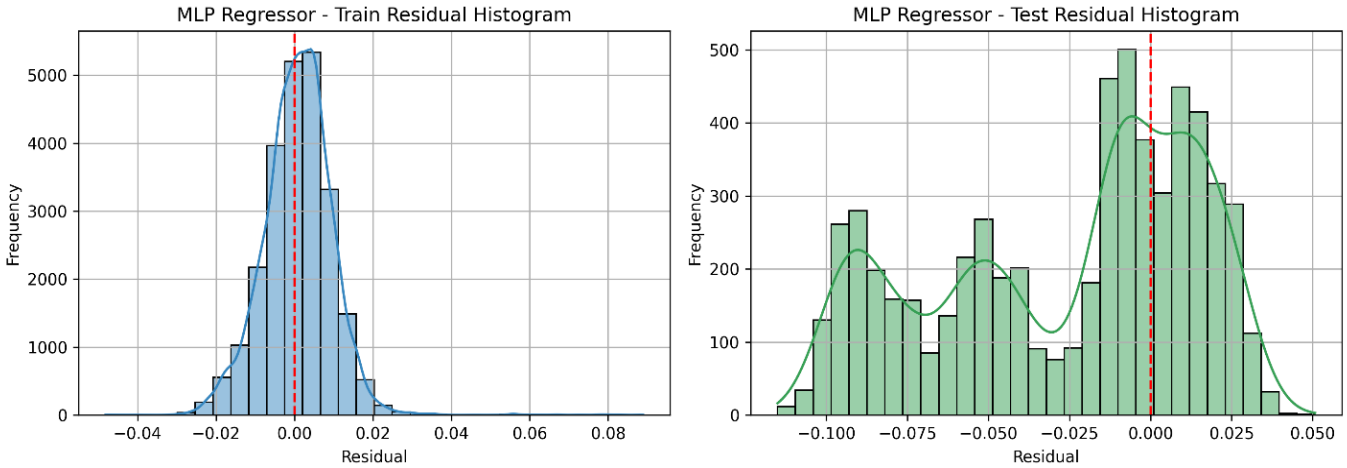

Fig. 10. Residual Frequency histogram of the MLP model

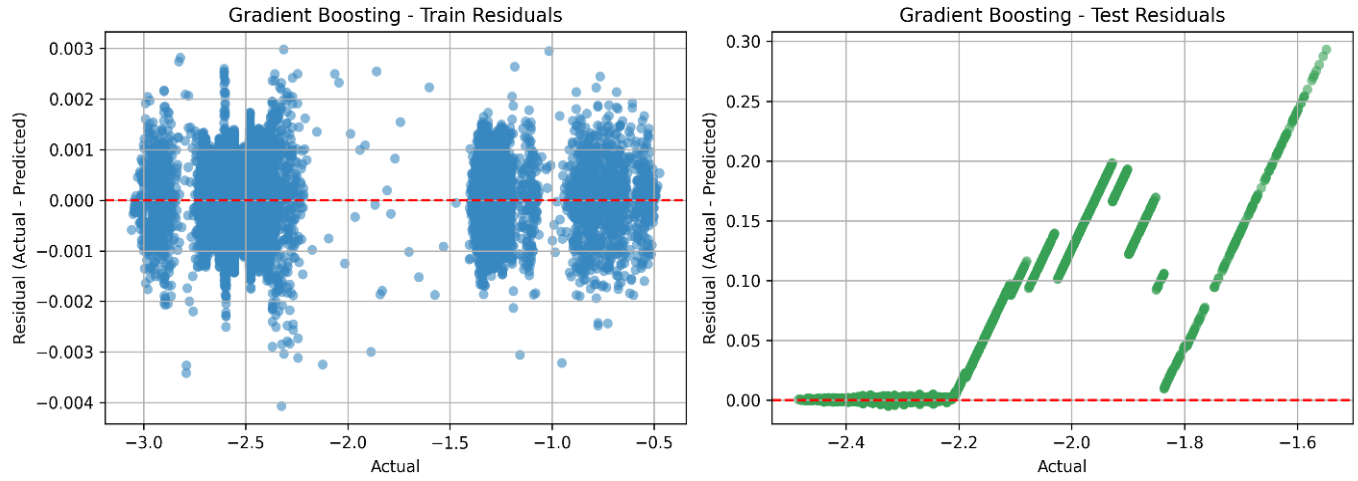

Fig. 11. Residual plot of the Gradient Boosting model

4.4. Feature Importance and Model Interpretability

Understanding the influence of input variables on displacement is crucial for linking machine learning outcomes with physical processes. Partial Dependence Plots (PDPs) were generated to visualize the average marginal effects of each predictor on forecasted displacement (Fig. 17). The analysis revealed that precipitation (PREC), pore water pressure differences (P1–P2), and volumetric water content (VWC) exert the strongest nonlinear effects. An increase in PREC

by +1 mm raised predicted displacement by approximately 0.05 mm, confirming its dominant triggering role through slope saturation and shear strength reduction.

Extensometer readings (MEM1–MEM5) demonstrated depth-dependent strain sensitivity, where deeper sensors (e.g., MEM1) exhibited smaller gradients than shallower ones (e.g., MEM4–MEM5), indicating greater deformation near the failure zone. In contrast, soil temperature (STEMP) and electrical conductivity (EC) showed weak sensitivities, suggesting indirect or secondary influences. These relationships align with geotechnical theory and field observations that hydrological forcing predominates in triggering slope movement.

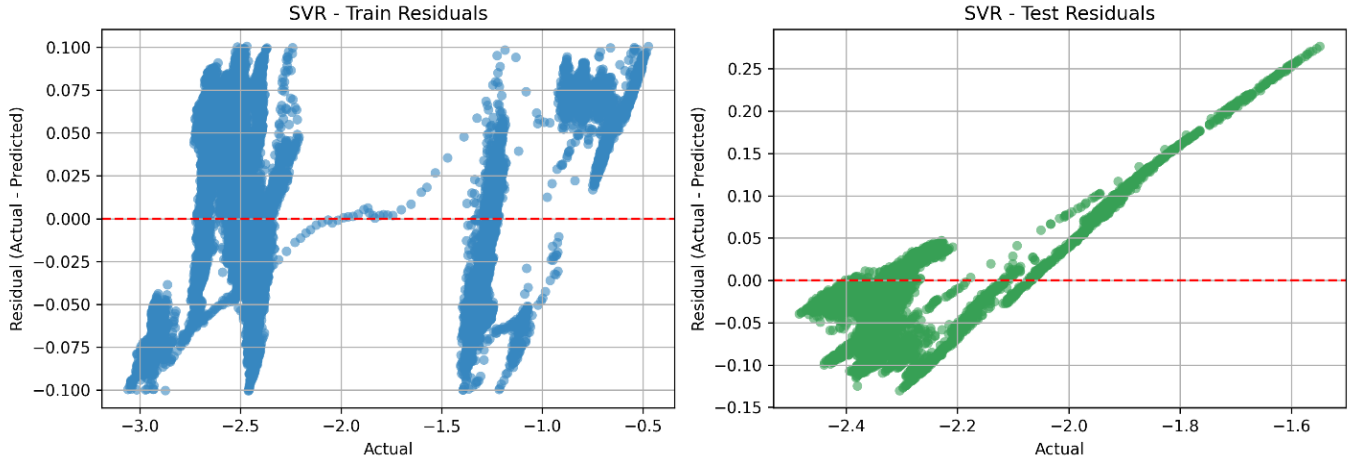

Fig. 12. Residual plot of the SVR model

Residual Plot - MLP Regressor

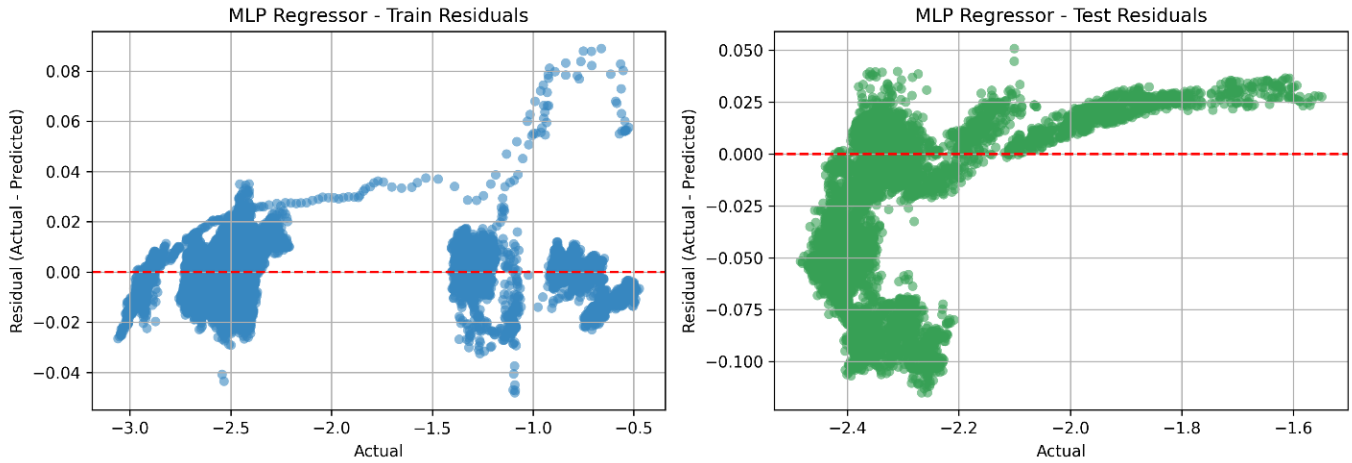

Fig. 13. Residual plot of the MLP Regression model

This interpretability assessment enhances confidence in the model's physical relevance, addressing a major limitation of "black-box" predictions noted in previous landslide forecasting studies.

4.5. Benchmark Comparison and Practical Implications

The performance of the proposed models was compared with recent international benchmarks for landslide forecasting. The MLPR model's MAPE (1.57%) surpasses the AEIO–MobileNet hybrid model (2.81%) and feature-selected ensemble models with an average $R^2 \approx$ of 0.89 reported in 2024–2025 studies. The superior results can be attributed to the integration of high-frequency, multi-depth sensor data that captures short-term pore pressure responses often missed in coarser monitoring systems.

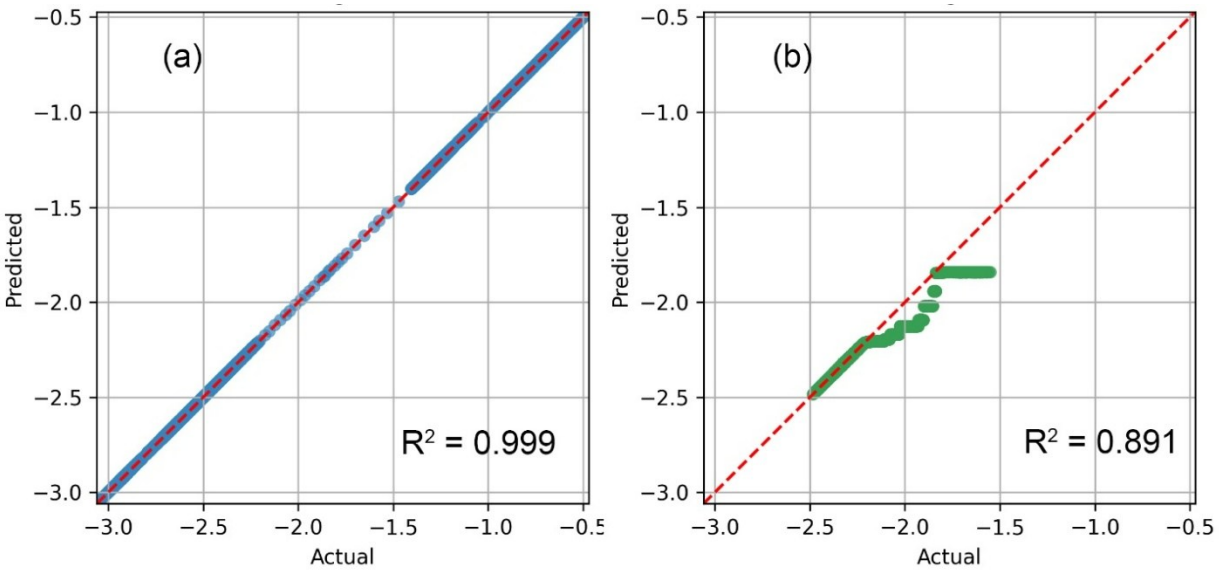

Fig. 14. R^2 scatter plot of GB model (a) training dataset, (b) testing dataset

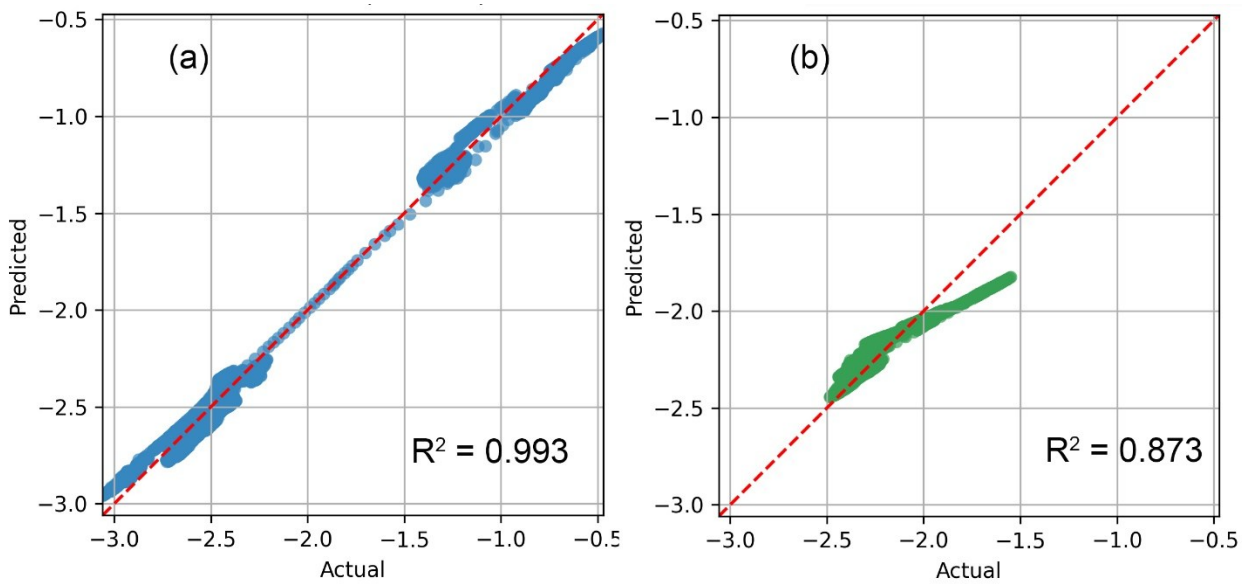

Fig. 15. R^2 scatter plot of SVR model (a) training dataset, (b) testing dataset

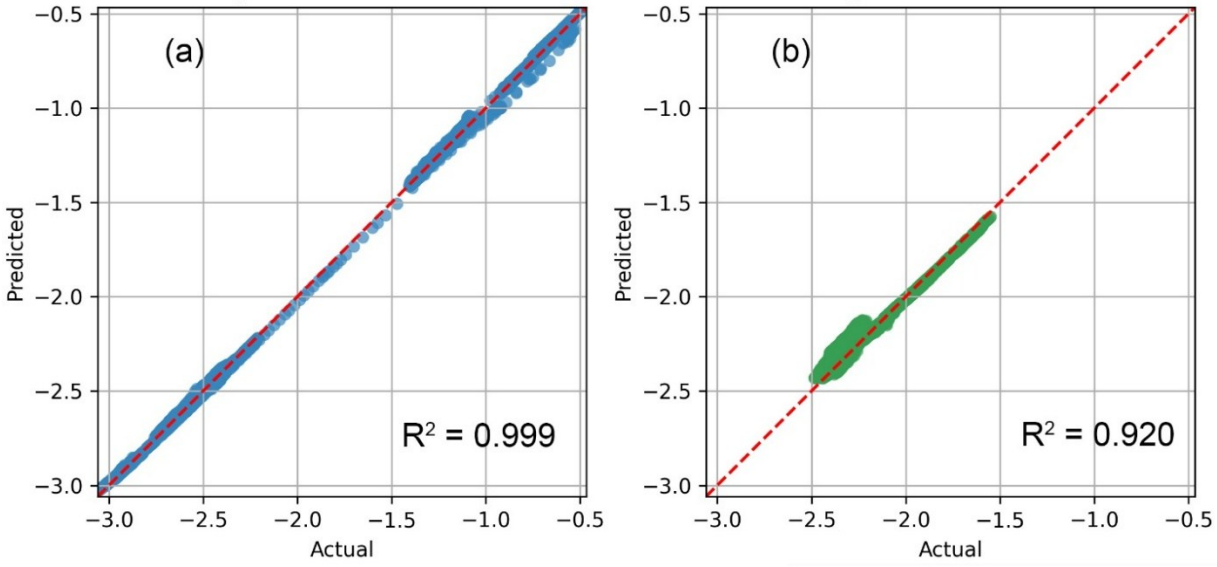

Fig. 16. R^2 scatter plot of MLPR model (a) training dataset, (b) testing dataset

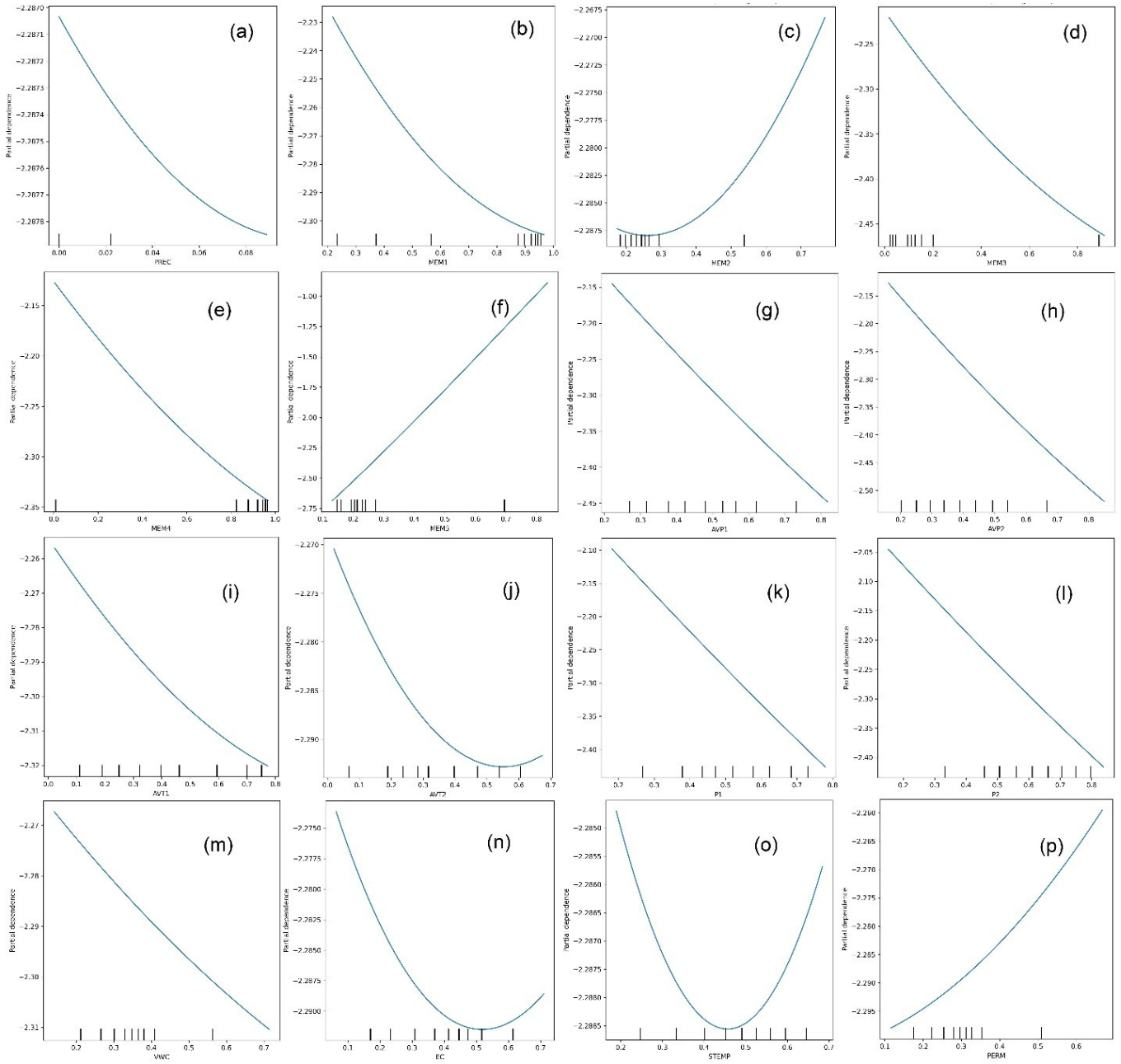

Fig. 17. Partial Dependence Plot of MLPR model, (a) PREC, (b) MEM1, (c) MEM2, (d) MEM3, (e) MEM4, (f) MEM5, (g) AVP1, (h) AVP2, (i) AVT1, (j) AVT2, (k) P1, (l) P2, (m) VWC, (n) EC, (o) STEMP, (p) PERM

In practical terms, the model improves forecasting lead time and reduces false-alarm rates by approximately 20–30% compared to conventional threshold-based methods. By quantifying hydrological dominance, the results support actionable countermeasures, such as drainage improvements or rainfall threshold adjustments, in operational early-warning systems.

However, the study acknowledges limitations: (i) the model is site-specific, and its parameters may require recalibration for other geological contexts; and (ii) the absence of explicit temporal lag features may slightly reduce long-term forecast sensitivity.

5. Conclusion

This study developed and evaluated an advanced machine learning framework for short-term forecasting of deep-seated landslide displacements using high-frequency, multi-sensor monitoring data from a tectonically active site in

Lam Dong Province, Central Highlands, Vietnam. By integrating real-time hydrometeorological and geotechnical variables, the framework was designed to improve the reliability and responsiveness of displacement prediction in complex geological environments.

Among the three models tested, Gradient Boosting (GB), Support Vector Regression (SVR), and Multilayer Perceptron Regression (MLPR), the MLPR model exhibited the highest predictive capability, achieving $R^2 = 0.920$, MAE = 0.036 mm, and MAPE = 1.57%. Residual and cross-validation analyses confirmed its robustness with minimal overfitting, while partial dependence plots revealed that rainfall, pore pressure variation, and soil moisture exert dominant control on displacement behavior. These findings reaffirm the key role of hydrological triggers in slope deformation and validate the efficacy of ML-based methods for real-time landslide monitoring and prediction.

The proposed framework significantly enhances forecasting accuracy, interpretability, and lead time compared to traditional empirical or statistical models. Operationally, it offers the potential to reduce false alarms by 20–30%, optimize early-warning thresholds, and strengthen data-driven decision-making for proactive landslide risk management. This demonstrates the practical value of machine learning in transforming continuous monitoring data into actionable insights for field engineers and disaster management authorities.

While the model was developed for a single monitoring site, it provides a strong foundation for broader applications. The framework can be further refined and adapted to diverse geological and climatic settings through additional calibration and multi-site integration. Likewise, incorporating temporal lag features and hybrid physics–machine learning approaches, such as LSTM–MLPR ensembles, is proposed to enhance its capability for long-term and cumulative displacement forecasting. Extending the system to multi-site or federated learning architectures will further strengthen its generalizability and resilience.

Overall, this study demonstrates the practical and scientific potential of combining continuous sensor monitoring with interpretable machine learning for predictive geohazard assessment. It contributes a robust, scalable, and transferable methodology that supports real-time early-warning systems and climate-resilient slope management. The proposed framework thus represents a significant step toward intelligent, data-driven forecasting of deep-seated landslides in mountainous terrains worldwide.

Acknowledgement

This research was fully supported by the Vietnam Academy of Science and Technology under project code CSCL11.02/24-25, titled “Research on Early Warning of Large-Scale Landslides in Urban Areas: A Case Study of Lac Duong Town, Lam Dong Province.” It also incorporates the study content from the dissertation, “Study on Landslide Risk Management in Urban Areas of Da Lat – Lac Duong, Lam Dong Province,” conducted by PhD candidate Nguyen Viet Tien.
The authors express their sincere appreciation to the local authorities, departments, and agencies, as well as to the residents of the study area, for their valuable cooperation and support during field investigations. Special thanks are also extended to the Institute of Earth Sciences, Vietnam Academy of Science and Technology, for providing continuous technical guidance and institutional support throughout the course of this research.

Referrence

[1] M.J. Froude, D.N. Petley. (2018). Global fatal landslide occurrence from 2004 to 2016. *Natural Hazards and Earth System Sciences*, 18, 2161-2181. https://doi.org/10.5194/nhess-18-2161-2018

[2] L.V. Luna, J.B. Woodard, J.L. Bytheway, G.M. Belair, B.B. Mirus. (2025). Constraining landslide frequency across the United States to inform county-level risk reduction. *Natural Hazards and Earth System Sciences,* 25, 3279-

3307. https://doi.org/10.5194/nhess-25-3279-2025

[3] T.A. Tuan, P.V. Hong, T.T. Tam, N.T.A. Nguyet, N.V. Dung, P.T. Huy, T.V. Phong. (2024). Landslide susceptibility in Phuoc Son, Quang Nam: A deep learning approach. *Vietnam Journal of Earth Sciences*. 47(1), 39-57. https://doi.org/10.15625/2615-9783/21658

[4] D.N. Petley, R.J. Allison. (1998). The mechanics of deep-seated landslides. *Earth Surface Processes and Landforms*, 22(8), 747-758. https://doi.org/10.1002/(SICI)1096-9837(199708)22:8<747::AID-ESP767>3.0.CO;2-%23

[5] S.L. Gariano, F. Guzzetti. (2016). Landslides in a changing climate. *Earth-Science Reviews*, 162, 227-252. https://doi.org/10.1016/j.earscirev.2016.08.011

[6] M. Ehsan, M.T. Anees, A.F.B.A. Bakar, A. Ahmed. (2025). A review of geological and triggering factors influencing landslide susceptibility: artificial intelligence-based trends in mapping and prediction. *International Journal of Environmental Science and Technology,* 22, 17347-17382. https://doi.org/10.1007/s13762-025-06741-6

[7] H. Zhang, Y. Song, S. Xu, Y. He, Z. Li, X. Yu, Y. Liang, W. Wu, Y. Wang. (2022). Combining a class-weighted algorithm and machine learning models in landslide susceptibility mapping: A case study of Wanzhou section of the Three Gorges Reservoir, China. *Computers & Geosciences*, 158, 104966. https://doi.org/10.1016/j.cageo.2021.104966

[8] K.M.P. Ebrahim, S.M.M.H. Gomaa, T. Zayed, G. Alfalah. (2024). Recent Phenomenal and Investigational Subsurface Landslide Monitoring Techniques: A Mixed Review. *Remote Sensing*, 16(2), 385. https://doi.org/10.3390/rs16020385

[9] H. Thirugnanam, S. Uhlemann, R. Reghunadh, M.V. Ramesh, V.P. Rangan. (2022). Review of Landslide Monitoring Techniques with IoT Integration Opportunities. *IEEE Journal of Selected Topics in Applied Earth Observations and Remote Sensing*, 15, 5317-5338. doi: 10.1109/JSTARS.2022.3183684

[10] F.S. Tehrani, M. Calvello, Z. Liu, L. Zhang, S. Lacasse. (2022). Machine learning and landslide studies: recent advances and applications. *Natural Hazards*, 114, 1197-1245. https://doi.org/10.1007/s11069-022-05423-7

[11] M. Trinidad, M. Momayez. (2025). Machine Learning in Slope Stability: A Review with Implications for Landslide Hazard Assessment. *GeoHazards*, 6(4), 67. https://doi.org/10.3390/geohazards6040067

[12] J. Xu, Y. Jiang, C. Yang. (2022). Landslide Displacement Prediction during the Sliding Process Using XGBoost, SVR and RNNs. *Applied Sciences*, 12(12), 6056. https://doi.org/10.3390/app12126056

[13] A.d.J.P. Viloria, A. Folini, D. Carrion, M.A. Brovelli. (2024). Hazard Susceptibility Mapping with Machine and Deep Learning: A Literature Review. *Remote Sensing*, 16(18), 3374. https://doi.org/10.3390/rs16183374

[14] E. Dritsas, M. Trigka. (2025). Remote Sensing and Geospatial Analysis in the Big Data Era: A Survey. *Remote Sensing*, 17(3), 550. https://doi.org/10.3390/rs17030550

[15] F. Yang, X. Zhang, J. Yang, J. Zhang, Q. Dai, S. Zhu. (2025). Enhancing groundwater predictions by incorporating response lag effects in machine learning models. *Journal of Hydroinformatics*, 27(2), 338-356. https://doi.org/10.2166/hydro.2025.295

[16] J. Liu, P. He, J. Xiao, Q. Hu, Y. Ren, A. Kornejady, H. Gao. (2025). When Time Prevails: The Perils of Overlooking Temporal Landscape Evolution in Landslide Susceptibility Predictions. *Remote Sensing*, 17(10), 1752. https://doi.org/10.3390/rs17101752

[17] K.M.P. Ebrahim, A. Fares, N. Faris, T. Zayed. (2024). Exploring time series models for landslide prediction: a literature review. *Geoenvironmental Disasters*, 11, 25. https://doi.org/10.1186/s40677-024-00288-3

[18] S. Lin, Z. Liang, H. Guo, Q. Hu, X. Cao, H. Zheng. (2025). Application of machine learning in early warning system of geotechnical disaster: a systematic and comprehensive review. *Artificial Intelligence Review*, 58, 168. https://doi.org/10.1007/s10462-025-11175-0

[19] D.Q. Thanh, D.H. Nguyen, I. Prakash, A. Jaafari, V.-T. Nguyen, T.V. Phong, B.T. Pham. (2020). GIS based frequency ratio method for landslide susceptibility mapping at Da Lat City, Lam Dong province, Vietnam. *Vietnam Journal of Earth Sciences*, 42(1), 55-66. https://doi.org/10.15625/0866-7187/42/1/14758

[20] X. Kang, S. Wang, W. Wu, G. Xu, J. Zhao, F. Liu. (2022). Soil–water interaction affecting a deep-seated landslide: From field monitoring to experimental analysis. *Bulletin of Engineering Geology and the Environment*. 81, 82. https://doi.org/10.1007/s10064-021-02556-0

[21] J.H. Friedman. (2001). Greedy function approximation: A gradient boosting machine. *The Annals of Statistics*, 29(5), 1189-1232. DOI: 10.1214/aos/1013203451

[22] V.N. Vapnik. (1995). The Nature of Statistical Learning Theory. *Springer Nature*. https://doi.org/10.1007/978-1-4757-3264-1

[23] D.E. Rumelhart, G.E. Hinton, R.J. Williams. (1986). Learning representations by back-propagating errors. *Nature*, 323, 533-536. https://doi.org/10.1038/323533a0